

Numerical Study of the H^0 Atomic Density and the Balmer Line Intensity Profiles in a Hydrogen Negative Ion Source with the Effect of Non-Equilibrium Electron Energy Distribution Function

Takanori SHIBATA, Mieko KASHIWAGI¹⁾, Akiyoshi HATAYAMA,
Keiji SAWADA²⁾, Takashi INOUE¹⁾ and Masaya HANADA¹⁾

Keio University, 3-14-1 Hiyosi, Yokohama, Kanagawa 223-8522, Japan

¹⁾*Japan Atomic Energy Agency, 801-1 Mukouyama, Naka, Ibaraki 311-0193, Japan*

²⁾*Shinshu University, 4-17-1 Wakasato, Nagano 380-8553, Japan*

(Received 22 November 2013 / Accepted 31 December 2013)

Spatial profiles of the atomic (H^0) density and the resultant H_α line intensity are investigated in a large negative ion source (the Japan Atomic Energy Agency (JAEA) 10 A negative ion source). The H^0 density analysis has been done in the present study with the effects of production, transport, and ionization processes by taking into account the non-Maxwellian component of electron energy distribution function (EEDF). The H^0 density profile shows a non-uniform spatial profile due to the local enhancement of the H^0 production rate even with the flattening effects by the ionization and the transport processes. The H_α line intensity observed from the viewing ports in the spectrometry is compared with the line intensity in the calculation to validate the numerical results. The both results show a good agreement in the spatial profile. It has been shown that the non-Maxwellian component of the EEDF plays an important role to determine the profile of the H_α line intensity in the plasma production region.

© 2014 The Japan Society of Plasma Science and Nuclear Fusion Research

Keywords: negative ion source, spatial non-uniformity of atomic density, numerical analysis, electron energy distribution function, atomic transport, Collisional-Radiative model

DOI: 10.1585/pfr.9.1401011

1. Introduction

To develop the negative ion based neutral beam injector system for fusion devices such as JT-60SA [1], the understandings for the non-uniformity of large negative ion sources have been one of the most serious problems to obtain sufficient injection power in fusion plasmas. It was observed in the Japan Atomic Energy Agency (JAEA) 10 Ampere negative ion source (10 A source) [2] that a high intensity negative ion beam was extracted from a high electron temperature (T_e) region (~ 4 eV) under the Cs-seeded condition. Since the negative ions are considered to be produced from the atoms in the Cs-seeded negative ion source [3], it has been shown that the local enhancement of the atomic (H^0) density due to high- T_e in the driver region and the resultant non-uniform H^0 flux to the plasma grid are possible origins of the H^- beam non-uniformity in the 10 A source [4]. The local enhancement of the H^0 density is mainly due to the enhancement of the dissociation for H_2 molecules which results in the H^0 production.

Recently, it has been reported in Ref. [5] that the spatial profile of H^0 production rate has been calculated with the effect of the non-Maxwellian EEDF in the 10 A source. In addition, the spatial profile of the H^0 production rate has a strong correlation with that of the H_α line intensity

obtained by the spectrometry. From the comparison, it has been suggested that the high energy tail of the EEDF enhances the non-uniformity of the H^0 production. However, not only the effect of H^0 production, but also the effect of transport and ionization loss of H^0 atoms should be taken into account to calculate directly the H^0 density. It is also important to evaluate the H^0 density for the direct comparison of the numerical results with the H_α line intensity by spectrometry.

The purpose of this study is to obtain the H^0 density with the effects of transport and ionization processes, and to compare directly the numerical results of H_α line intensity with that by experiments. For this purpose, firstly, atomic transport analysis which takes into account the non-Maxwellian EEDF and the resultant ionization processes is developed to obtain the spatial profile of the H^0 density. Moreover, a Collisional-Radiative (CR) model is also developed to obtain the population ratio of excited atoms and the resultant H_α line intensity with the effect of non-Maxwellian EEDF.

2. Experimental Setup of Spectrometry and Spatial Profile of H^0 Production Rate in Previous Study

Before going to the numerical analysis, here, we

author's e-mail: shibata@ppl.appi.keio.ac.jp

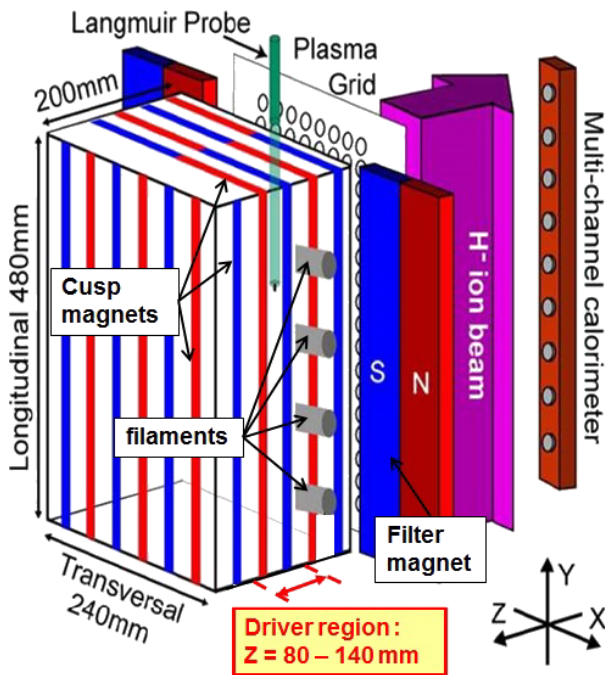


Fig. 1 Schematic drawing of the JAEA 10 ampere (10 A) negative ion source; cited from Ref. [5].

briefly summarize the JAEA 10 A source [2] and experimental setup for the H_{α} measurement. Figure 1 shows a schematic drawing of the 10 A negative ion source. Hydrogen plasma is produced by arc discharge between the rectangular source chamber (anode) and tungsten filament cathodes installed in the longitudinal direction. The dimension of the source chamber is 240 mm in the transverse direction (X), 480 mm in the longitudinal direction (Y) and 200 mm in depth (Z). The discharge conditions in the present study have been fixed as following values; arc power: 10 kW, arc voltage: 60 V, arc current: 166.7 A, and H_2 gas pressure: 0.30 Pa.

As shown in Fig. 2, eight viewing ports for spectrometry are located along the Y direction on the side walls at $Z = 81$ mm in the axial direction (in the driver region). Each viewing port has same viewing angles with ± 5 degrees. The line intensity obtained at each port is an integrated value along the line of sight inside the viewing angles.

Figure 3 shows the comparison between the H_{α} line intensity obtained in the spectrometry and the calculated H^0 production rate in Ref. [5]. The H^0 production profile calculated with the non-Maxwellian component of the EEDF has a strong correlation with that of the H_{α} line intensity. As was discussed in Ref. [5], however, the effect of the transport and the ionization loss of H^0 atoms should be taken into account to calculate the H^0 density, since the calculation of the H^0 density is required for the direct comparison of H_{α} line intensity between the spectrometry and the numerical analysis.

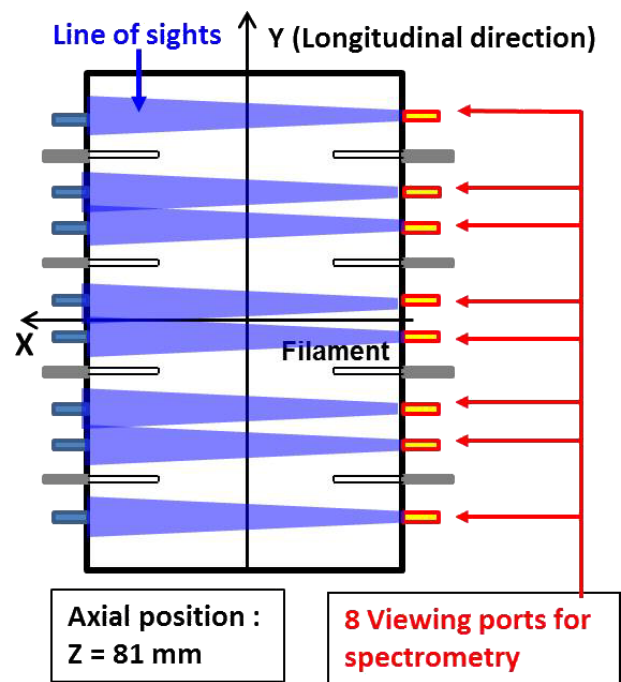


Fig. 2 Schematic diagram of spectrometry in the 10 A source (XY plane).

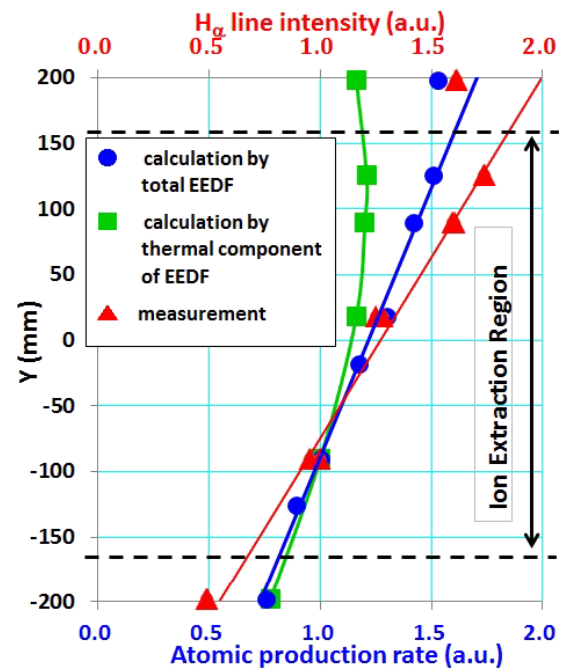


Fig. 3 Spatial profiles of the calculated H^0 production rate from the total EEDF (blue circles), the calculated H^0 production rate with only the thermal electron component ($\epsilon < 25$ eV) of the EEDF (green squares) and measured H_{α} line intensity (red triangles); cited from Ref. [5].

3. Atomic Density Analysis

First, the details of the atomic transport analysis are shown. The H^0 density is calculated from the Boltzmann

equation, which describes the H^0 distribution function $f_H(\mathbf{r}, \mathbf{v}_H, t)$ over position, \mathbf{r} , atomic velocity, \mathbf{v}_H , space and time t ,

$$\partial f_H(\mathbf{r}, \mathbf{v}_H, t) / \partial t + \mathbf{v}_H \cdot \nabla f_H(\mathbf{r}, \mathbf{v}_H, t) = C(f_H). \quad (1)$$

The H^0 density at each position can be calculated by integrating distribution function in the velocity space, as $n_H(\mathbf{r}) = \int f_H(\mathbf{r}, \mathbf{v}_H) d\mathbf{v}_H$.

In the collision term, we may include the following three effects; (1) H^0 production (S_{PROD}), (2) loss due to ionization (S_{IO}) and (3) momentum transfer due to charge exchange (S_{CX}) as,

$$C(f_H) = S_{\text{PROD}} - S_{\text{IO}} + S_{\text{CX}}. \quad (2)$$

The H^0 production term S_{PROD} is given by $S_{\text{PROD}} = S_{\text{DISS}}(\mathbf{r})\delta(v_H - v_0)/4\pi$, where $v_0 = \sqrt{2E/m_H}$, E and m_H are velocity, energy and mass of hydrogen atom, respectively. The produced atoms are assumed to be Franck-Condon atoms which have initial energy $E = 2.15$ eV and have isotropic velocity distribution. The dissociation rate $S_{\text{DISS}}(\mathbf{r})$ above is,

$$S_{\text{DISS}}(\mathbf{r}) = \int f_{H_2}(\mathbf{r}, \mathbf{v}_{H_2}) \int \|\mathbf{v}_{H_2} - \mathbf{v}_e\| \sigma_{\text{DISS}} \times f_e(\mathbf{r}, \mathbf{v}_e) d\mathbf{v}_e d\mathbf{v}_{H_2}, \quad (3)$$

where \mathbf{v}_{H_2} , \mathbf{v}_e , σ_{DISS} are velocities of H_2 molecules and electrons, and cross-section for dissociation processes. The distribution functions of molecules is denoted as $f_{H_2}(\mathbf{r}, \mathbf{v}_{H_2})$ which is assumed to be Maxwellian distribution function with molecular temperature 1000 K and density $2.83 \times 10^{19} \text{ m}^{-3}$ as in Ref. [5]. The electron distribution function $f_e(\mathbf{r}, \mathbf{v}_e)$ is equivalent with the EEDF which has been obtained in electron transport analysis shown in Ref. [6, 7].

The terms for ionization loss rate, S_{IO} , and charge exchange rate, S_{CX} , are described, respectively, as follows;

$$S_{\text{IO}} = f_H(\mathbf{r}, \mathbf{v}_H) \int \|\mathbf{v}_H - \mathbf{v}_e\| \sigma_{\text{IO}} f_e(\mathbf{r}, \mathbf{v}_e) d\mathbf{v}_e, \quad (4)$$

$$S_{\text{CX}} = f_i(\mathbf{r}, \mathbf{v}_H) \int \|\mathbf{v}_H - \mathbf{w}_H\| \sigma_{\text{CX}} f_H(\mathbf{r}, \mathbf{w}_H) d\mathbf{w}_H - f_H(\mathbf{r}, \mathbf{v}_H) \int \|\mathbf{v}_H - \mathbf{v}_i\| \sigma_{\text{CX}} f_i(\mathbf{r}, \mathbf{v}_i) d\mathbf{v}_i, \quad (5)$$

where \mathbf{w}_H , \mathbf{v}_i , σ_{IO} and σ_{CX} are H^0 velocity before collision, ion (H^+) velocity and the cross-sections of ionization and charge exchange, respectively. The ion distribution function is assumed to be spatially uniform Maxwellian distribution function with ion temperature 1000 K and density 10^{18} m^{-3} . As mentioned in Ref. [8], the ion temperature is considered to be in the range between gas temperature (1000 K) and Franck-Condon energy of atoms. We have simply assumed the ion temperature to be equal to the gas temperature as an initial calculation.

Based on the test particle model, we solve the Boltzmann equation (Eq. (1)). In the model the test particle trajectories are directly followed by numerically solving their equations of motion, which is equivalent to solve

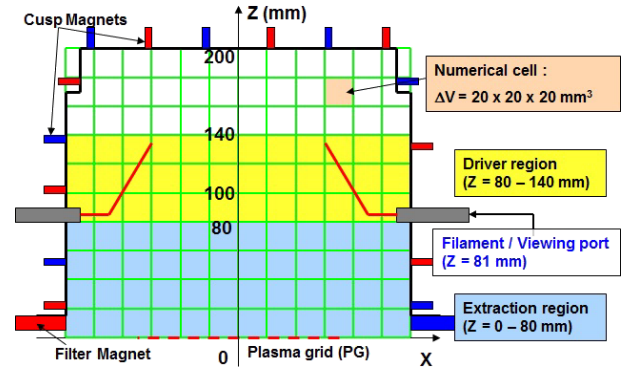


Fig. 4 Geometry of the 10 A source in XZ plane and numerical cells.

the Boltzmann equation. For the collision term $C(f_H)$ on the right-hand side of Eq. (1), we applied the Monte-Carlo method [9]. In addition, the particle and energy reflection coefficients for test particles which reach the wall are included in the analysis as in the same manner with those in Ref. [4, 10, 11]. Moreover, test particles which reach the extraction aperture are removed from the calculation. The production rate of the test particles and the initial position are determined from the production rate S_{PROD} in the real system. Each test particle has a weight $\omega = 1.0 \times 10^{10}$. As shown in Fig. 4, the source chamber of the 10 A source is divided into total 2880 numerical cells with volume $\Delta V = 20 \text{ mm} \times 20 \text{ mm} \times 20 \text{ mm}$. After reaching a quasi-steady state, the total number of test particles in each cell, N_T , is counted to calculate H^0 density as $n_H = N_T \times \omega / \Delta V$. The size of the cell is smaller compared with mean free paths of ionization and charge exchange of H^0 atoms (both are up to 0.1 - 1 m) which have largest reaction rates.

In the present model, transport process of atoms is solved by Boltzmann equation without separating the excited levels. It is considered that the population density ratio of each excited atom is immediately decided by collision processes after the total density for all excited levels of atom is decided at each position by transport process. The reason we have separated calculations of the two processes (atomic transport process and transition of excited levels due to collision processes) is that the time scales of the collision processes and the transport process is much different for atoms. As mentioned in Ref. [12], the characteristic time scale of reaction processes which decide the population density ratio of excited atoms is up to 10^{-8} s while time scale of the transport is 10^{-4} - 10^{-5} s which is estimated to be the characteristic time scale of atoms to across the negative ion source chamber (the size of the source chamber is $L \sim 0.1$ m and the atomic speed is 10^3 - 10^4 m/s). In that case, the separation principle can be applied. The population density calculation for each excited level is shown as follows.

From the H^0 density distribution obtained from the transport analysis, the H_α line intensity is calculated by

the CR model [8, 13]. As shown in Ref. [8, 13], the H_α line emission rate ε_{H_α} ($\text{m}^{-3} \text{s}^{-1}$) in the driver region of negative ion sources is mainly described as,

$$\varepsilon_{H_\alpha} = n_H n_e \left\{ X_{H_\alpha}^{\text{eff,H}} + (n_{H_2}/n_H) X_{H_\alpha}^{\text{eff,H}_2} \right\}, \quad (6)$$

with the usage of an effective emission rate coefficient for H^0 and H_2 ,

$$X_{H_\alpha}^{\text{eff,H}} = A_H(3, 2)R_H(3), \quad X_{H_\alpha}^{\text{eff,H}_2} = A_H(3, 2)R_{H_2}(3), \quad (7)$$

respectively. The coefficient $A_H(3, 2)$ represents the spontaneous transition probability of atomic hydrogen from the excited level 3 to 2. The population coefficients $R_s(p)$ (s denotes the particle species; $s = H, H_2$) are the ratio of excited atoms with excited level $p = 3$ to the total density of all excited states. Therefore, the coefficients are denoted as $R_s(p) = n_H(p) / \sum_q n_s(q)$ where $n_s(p)$ and $n_s(q)$ are the population density in excited level p and q , respectively. The population densities and the population coefficients are calculated in the CR model as in the same manner as in Ref. [8, 13] from the rate equations,

$$\begin{aligned} dn_{H_2}(p)/dt = & \left[\left\{ \sum_{q<p} C_{H_2}(q, p) + \sum_{q>p} F_{H_2}(q, p) \right\} n_e \right. \\ & + \left. \sum_{q>p} A_{H_2}(q, p) \right] n_{H_2}(q) - \left[\left\{ \sum_{q<p} C_{H_2}(q, p) \right. \right. \\ & + \left. \left. \sum_{q>p} F_{H_2}(q, p) + S_{H_2}(p) + D_{H_2}^H(p) \right\} n_e \right. \\ & + \left. \left. \sum_{q>p} A_{H_2}(q, p) \right] n_{H_2}(p) \end{aligned} \quad (8)$$

$$\begin{aligned} dn_H(p)/dt = & \left[\left\{ \sum_{q<p} C_H(q, p) + \sum_{q>p} F_H(q, p) \right\} n_e \right. \\ & + \left. \sum_{q>p} A_H(q, p) \right] n_H(q) - \left[\left\{ \sum_{q<p} C_H(q, p) \right. \right. \\ & + \left. \left. \sum_{q>p} F_H(q, p) + S_H(p) \right\} n_e \right. \\ & + \left. \left. \sum_{q>p} A_H(q, p) \right] n_H(p) + P_{H_2}^H(p) \end{aligned} \quad (9)$$

where $C_s(p, q)$, $F_s(p, q)$ and $S_s(p, q)$ are the rate coefficients for excitation, de-excitation and ionization transition from excited level p to q , respectively. The main reactions taken into account in this model are shown in Table 1 [13–18]. The rate coefficients are calculated by substituting the non-Maxwellian EEDF from the electron

Table 1 Main Reactions taken into account in the CR models. The excited levels for atoms and molecules are denoted by p and q .

#	Reaction	Reference
1 (H_2 excitation)	$H_2(p) + e \rightarrow H_2(q) + e$ ($p < q$)	[13, 14]
2 (H_2 de-excitation)	$H_2(p) + e \rightarrow H_2(q) + e$ ($p > q$)	[13]
3 (H_2 ionization)	$H_2(p) + e \rightarrow H_2^+ + e + e$	[13, 14]
4 (H_2 spontaneous radiation)	$H_2(p) \rightarrow H_2(q) + h\nu$ (line emission) ($p > q$)	[13, 14]
5 (H_2 dissociation ; Franck-Condon process)	$H_2(p) + e \rightarrow H(1s) + H(1s) + e$	[15]
6 (H_2 dissociative ionization)	$H_2 + e \rightarrow H(1s) + H^+ + e + e$	[16]
7 (H_2 dissociative excitation)	$H_2 + e \rightarrow H(1s) + H^*(p) + e$	[17, 18]
8 (H excitation)	$H(p) + e \rightarrow H(q) + e$ ($p < q$)	[14]
9 (H de-excitation)	$H(p) + e \rightarrow H(q) + e$ ($p > q$)	[14]
10 (H ionization)	$H(p) + e \rightarrow H^+ + e + e$	[14]
11 (H spontaneous radiation)	$H(p) \rightarrow H(q) + h\nu$ (line emission) ($p > q$)	[14]

transport analysis. The loss rate of $n_{H_2}(p)$ due to the dissociation is denoted as $D_{H_2}^H(p)$ and, conversely, the production rate of $n_H(q)$ due to dissociation is denoted as $P_{H_2}^H(q)$. From the above transport model (Boltzmann equation) and the CR model (rate equation), spatial distribution of population density for excited atom with principle number $p = 3$ ($H(3)$), which contributes to the H_α line emission, is numerically obtained. It has been reported in Ref. [19] that the H_α line intensity also shows strong correlation with the spatial distribution of the negative ion density in the extraction region (distance from the plasma grid to be $Z \lesssim 30$ mm) via Mutual Neutralization (MN) process in this region [20]. However, in the present analysis, we focus on the driver region ($Z > 80$ mm) for the reason mentioned in Sec. 1. In this region, the negative ion density is generally very low because of high electron temperature. Therefore, the production of H_α line emission in the driver region is mainly due to excitation, de-excitation, ionization and spontaneous radiation of atoms and dissociative excitation of molecules via electron impact (See Table 1). On other hand, the negative ion density is relatively large in the extraction region close to the PG. In the near future, H_α line emission in the extraction region will be studied by taking into account the MN process to the CR model.

4. Calculation Results

Figure 5 shows the spatial profile of atomic density in the XY plane of the driver region $Z = 90$ mm. As shown in the figure, even with the effects of ionization and transport, the H^0 density has a non-uniform profile. The high H^0 density is obtained in the upper region ($Y > 170$ mm) and

in the region near the filament cathodes inserted from the side walls. This is mainly due to the local enhancement of the H^0 production by the non-Maxwellian component of the EEDF (fast electrons), as shown in Ref. [5]. The spatial profiles of the fast electrons with kinetic energy 55 - 65 eV and the H^0 production rate in the XY plane of the driver region ($Z = 90$ mm) are shown in Figs. 6 and 7.

However, the H^0 density profile in Fig.5 shows weaker non-uniformity compared with the spatial profile of the H^0 production rate in Fig.7. This flattening of H^0

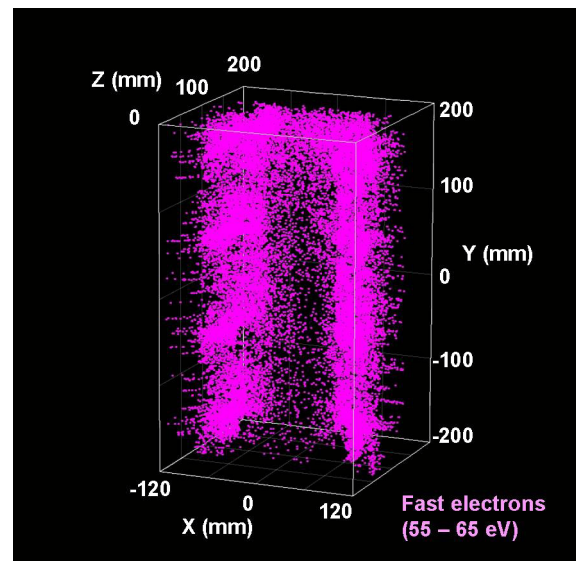


Fig. 6 Snapshot of fast electrons in the source chamber with kinetic energy 55 - 65 eV.

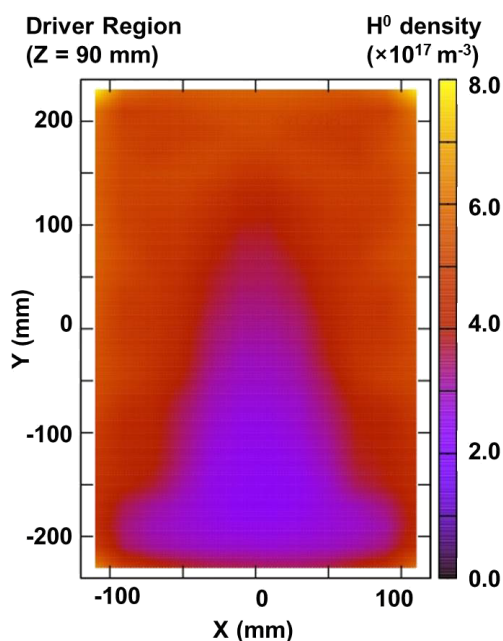


Fig. 5 Spatial profile of atomic density in the driver region; $Z = 90$ mm.

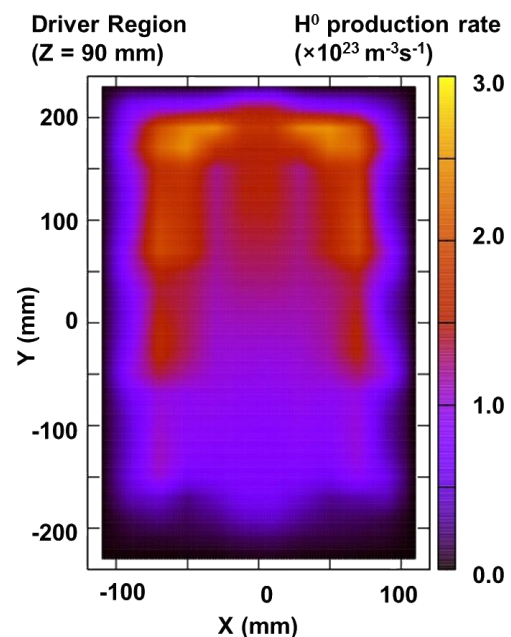


Fig. 7 Spatial profile of H^0 production rate in XY plane of the driver region.

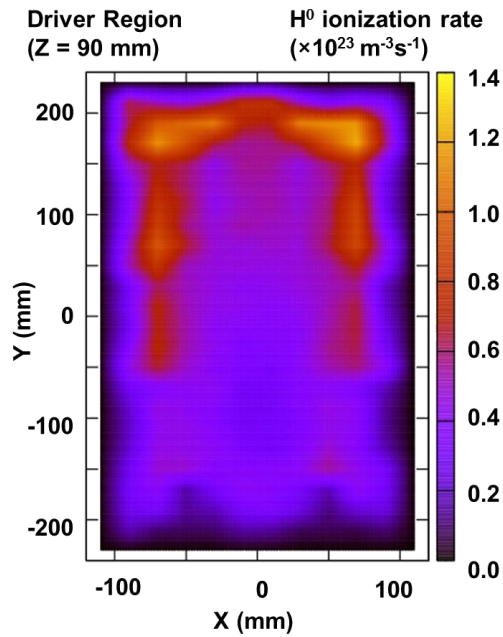


Fig. 8 Spatial profile of H^0 ionization rate in XY plane of the driver region.

density profile is mainly due to the effects of H^0 ionization loss and transport loss which are taken into account in the present analysis. As shown in Fig. 8, the ionization loss rate of H^0 shows large value in the region where the H^0 production rate is high. By this effect, the net production rate of H^0 becomes smaller (up to $\sim 70\%$ compared with the case without the effect of the ionization loss) in the upper region. As shown in Fig. 5, however, it is noticeable that the non-uniform spatial profile still takes place in the H^0 density even with the flattening due to the ionization and the transport effects.

Spatial profile of the H_α line emission rate calculated by the CR model is shown in Fig. 9. In comparison with the H^0 density profile, the H_α line emission profile has stronger non-uniformity with peaks at the region where the ratio of fast electrons is high. Figure 10 shows the typical EEDF in the upper end of the driver region ($Z = 90$ mm and $Y = 190$ mm) calculated in Ref. [7] and rate coefficients of dominant excitation processes for atomic production in excited state $p = 3$ which results in H_α line emission [13–18]. Although the excitation from the ground state atom (EXC) seems to have large cross-section than the dissociative excitation (DE) process, the DE rate is comparative with the atomic excitation rate because the H_2 density is up to 10^{19} m^{-3} . In the upper end of the driver region, the calculated EEDF has typically two components; (1) thermal component which obey Maxwellian distribution function decided from the electron temperature $T_e = 3 \text{ eV}$ and density $n_e = 3.0 \times 10^{18} \text{ m}^{-3}$, and (2) high energy tail component for electron energy larger than 20 eV. The Maxwellian distribution is also shown in Fig. 10 in solid line. It is noticeable that the high energy tail component has large contri-

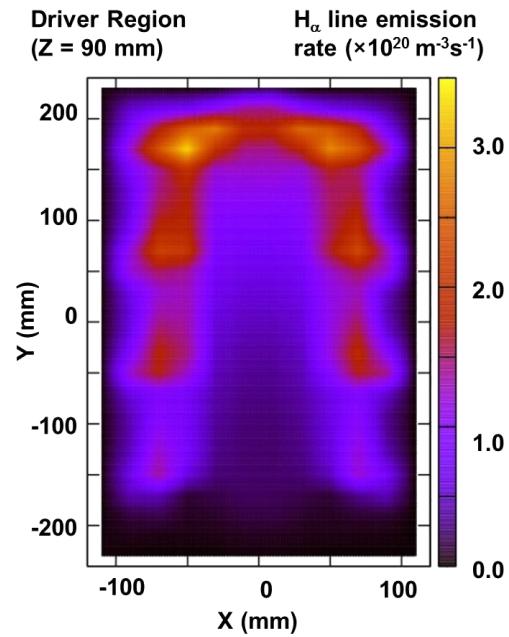


Fig. 9 Spatial profile of H_α line emission rate in XY plane of the driver region.

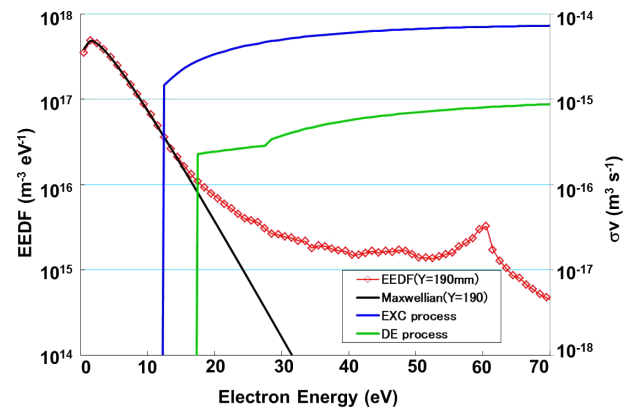


Fig. 10 Typical non-Maxwellian EEDF calculated in the driver region ($Z = 90$ mm and $Y = 190$ mm), Maxwellian distribution function with $T_e = 3 \text{ eV}$ and $n_e = 3.0 \times 10^{18} \text{ m}^{-3}$, rate coefficient of the electron impact excitation of atom from ground state (EXC) to excited state $p = 3$ and rate coefficient of the dissociative excitation of ground state molecule (DE) which produces atoms in excited level $p = 3$.

tribution to the both EXC and DE. This results in the high population ratio for excited atoms with principle number $p = 3$ and, therefore, the high H_α line intensity in the upper end of the driver region.

Figure 11 shows the H_α line intensity obtained in the spectrometry and in the calculation. The spatial (longitudinal) profile of the H^0 density averaged along the line of sight is also shown in the figure. The spatial profile of H_α line intensity calculated from the H^0 density profile (blue circles) is in the same order with that of the H_α line inten-

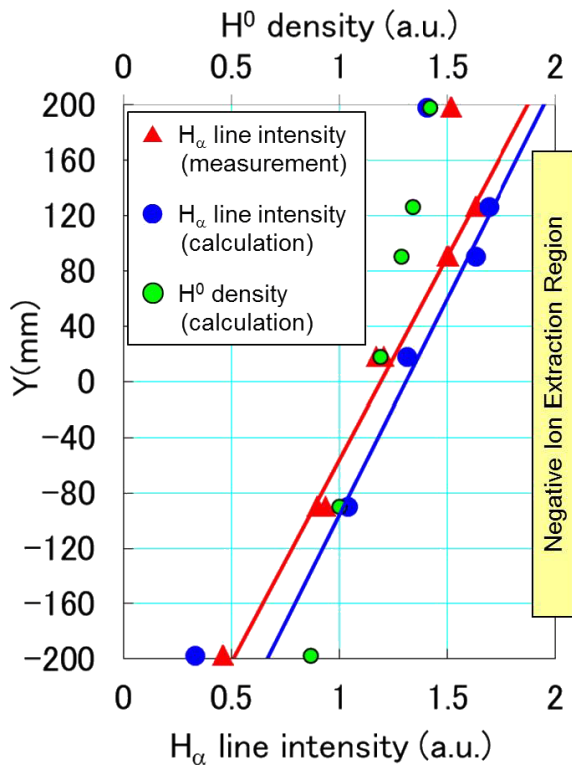


Fig. 11 Comparison of H_{α} line intensity observed from the viewing port in the spectrometry and in the present calculation.

sity obtained from the spectrometry (red triangles). The absolute values of the line intensity obtained in the calculation and in the spectrometry are both in the order of 10^{13} photons/s. On the other hand, spatial profile of the H^0 density is different from that of the H_{α} line intensity in the upper region. Moreover, non-uniformity of the H^0 density is weaker than that of the H_{α} line intensity in the negative ion extraction region ($Y = -170 - 170$ mm). This difference is due to the enhancement of the population ratio for $p = 3$ level by the non-Maxwellian component of EEDF as shown in Fig. 10.

5. Summary

The atomic (H^0) density profile has been obtained with the effects of transport, ionization processes and the non-Maxwellian component of EEDF. It has been shown that non-uniformity of the H^0 density profile in the driver region takes place due to the non-uniformity of the H^0 production rate even with the effect of flattening by transport and ionization loss.

From the H^0 density, the H_{α} line intensity profile which can be seen from each viewing port has been calculated in the driver region. The H_{α} line intensity obtained in the calculation shows a good agreement with that obtained in the spectrometry. It has been shown that the non-uniformity of the H_{α} line intensity is stronger than that of

the H^0 density profile. This is because the fast electrons with the energy larger than 20 eV enhances the excitation processes of ground state atoms and molecules which produces excited atoms with the principle number $p = 3$ and the resultant H_{α} line intensity.

From the non-uniformity of H^0 atoms, the surface production of the negative ion (H^-) and the resultant extraction physics of H^- will be investigated in the future to understand the H^- beam non-uniformity.

Acknowledgments

The authors are grateful to Prof. U. Fantz in Max-Planck-Institut für Plasmaphysik for the valuable discussions.

- [1] M. Kuriyama, N. Akino, T. Aoyagi, N. Ebisawa, N. Isozaki, A. Honda, T. Inoue, T. Itoh, M. Kawai, M. Kazawa, J. Koizumi, K. Mogaki, Y. Ohara, T. Ohga, Y. Okumura, H. Oohara, K. Ohshima, F. Satoh, T. Takenouchi, Y. Toyokawa, K. Usui, K. Watanabe, M. Yamamoto, T. Yamazaki and C. Zhou, *Fusion Eng. Des.* **39-40**, 115 (1998).
- [2] M. Hanada, T. Seki, N. Takado, T. Inoue, T. Mizuno, A. Hatayama, M. Kashiwagi, K. Sakamoto, M. Taniguchi and K. Watanabe, *Nucl. Fusion* **46**, S318 (2006).
- [3] Yu.I. Belchenko, G.I. Dimov and V.G. Dudnikov, *Investiya of USSR Academy of Science Ser. Fiz.* **37**, 2573 (1973).
- [4] N. Takado, H. Tobar, T. Inoue, J. Hanatani, A. Hatayama, M. Hanada, K. Kashiwagi and K. Sakamoto, *J. Appl. Phys.* **103**, 053302 (2008).
- [5] T. Shibata, M. Kashiwagi, T. Inoue, A. Hatayama and M. Hanada, *J. Appl. Phys.* **114**, 143301 (2013).
- [6] I. Fujino, A. Hatayama, N. Takado and T. Inoue, *Rev. Sci. Instrum.* **79**, 02A510 (2008).
- [7] T. Shibata, R. Terasaki, M. Kashiwagi, T. Inoue, M. Dairaku, M. Taniguchi, H. Tobar, N. Umeda, K. Watanabe, K. Sakamoto and A. Hatayama, *Analysis of electron temperature distribution by kinetic modeling of electron energy distribution function in JAEA 10 ampere negative ion source: Proceedings of the 3rd International Symposium on Negative Ions, Beams and Sources, Jyväskylä, Finland, 3-7 September 2012 (University of Jyväskylä, Jyväskylä, 2012), pp.177-186.*
- [8] U. Fantz and D. Wunderlich, *New Journal of Physics* **8**, 301 (2006).
- [9] K. Nanbu, *IEEE Trans.* **28**(3), 971 (2000).
- [10] R.A. Langley, J. Bohdansky, W. Eckstein, P. Mioduszewski, J. Roth, E. Taglauer, E.W. Thomas, H. Verbeek and K.L. Wilson, *Nucl. Fusion, special issue on Data Compendium for Plasma-Surface Interactions IAEA, Vienna, 1984, p.12.*
- [11] R. Behrisch and W. Eckstein, *Physics of Plasma-Wall Interactions in Controlled Fusion* (NATO Advanced studies Institute, Series B: Physics Plenum, New York, 1986), Vol.131, p.413.
- [12] K. Miyamoto, Y. Ishii and A. Hatayama, *J. Appl. Phys.* **93**, 845 (2003).
- [13] K. Sawada and T. Fujimoto, *J. Appl. Phys.* **78**, 2913 (1995).
- [14] L.C. Johnson, *Astrophys. J.* **174**, 227 (1972).
- [15] R.K. Janev, D. Reiter and U. Samm, *Juelich Report No.JUEL-4105* (2003).

- [16] R. Celiberto, R.K. Janev, A. Laricchiuta, M. Capitelli, J.M. Wadehra and D.E. Atems, *At. Data Nucl. Data Tables* **77**, 161 (2001).
- [17] T. Fujimoto, K. Sawada and K. Takahata, *J. Appl. Phys.* **66**, 2315 (1989).
- [18] K. Sawada, K. Eriguchi and T. Fujimoto, *J. Appl. Phys.* **73**, 8122 (1993).
- [19] K. Ikeda, H. Nakano, K. Tsumori, M. Kasaki, K. Nagaoka, M. Osakabe, Y. Takeiri and O. Kaneko, *Plasma Fusion Res.* **8**, 1301036 (2013).
- [20] N. Takado, K. Miyamoto and A. Hatayama, *Rev. Sci. Instrum.* **77**, 1777 (2004).